INVESTIGATION OF THE OXYGEN CONTENT OF ADDITIVELY MANUFACTURED TOOL STEEL 1.2344

R. Dörfert[a], J. Zhang[b], B. Clausen[b], H. Freiße[a], J. Schumacher[b], F. Vollertsen[a, c]

[a] BIAS – Bremer Institut für angewandte Strahltechnik GmbH, Klagenfurter Str. 5, D-28359 Bremen, Germany [b] Leibniz-Institut für Werkstofforientierte Technologien – IWT, Badgasteiner Str. 3, D-28359 Bremen, Germany

[c] University of Bremen, Bibliothekstraße 1, D-28359 Bremen, Germany

Abstract

Laser Beam Melting (LBM) offers a high design flexibility and the possibility to create complex metal parts in small batch sizes efficiently. However, several questions regarding the mechanical properties are still not conclusively clarified. In general, the remaining degree of porosity is regarded as major indicator on the parts properties. Other properties such as the resulting residual stresses, the oxygen contents and possible contaminants of the powder or the influence of humidity are less often taken into consideration and difficult to measure. In this work, the mechanical properties for LBM generated specimens out of tool steel 1.2344 are investigated and compared to conventionally fabricated material. The quasi-static properties are comparable to conventionally fabricated materials, whereas a significant impact on the fatigue strength was observed together with a high oxygen content of 569 ppm, with significant oxygen peaks that can be allocated to the fractured area.

Introduction

The additive manufacturing (AM) of metal parts out of powder via Laser Beam Melting (LBM, also referred to as PBF or SLM®) offers high flexibility in terms of part design and complexity. Thus, in recent years the technology grows rapidly in the fields of distribution, acceptance, AM-machine sales and possible industrial applications [1]. Beside the identification of the right use case [2] the establishment of LBM-generated parts for industrial applications requires mechanical properties comparable to conventionally fabricated material and a reliable reproducibility. In general, the tensile and fatigue behavior are comparable to conventionally fabricated material but still limited by the LBM-generated rough surface and the present volume defects which decrease the achievable stress limit [3]. Volume defects are often initiation sites for cracks and are formed due to unmolten areas within the parts or insufficient connection between the layers as well as entrapped gas pores [4]. Furthermore, the high surface roughness of the LBM-parts leads to notch affects and thus initiation points for cracks due to high stress concentrations [5]. Hence, post processing of the LBM-parts is often mandatory to remove the high surface roughness and thus improve the mechanical properties significantly [6]. In addition to the present defects the LBM-process induces high residual stresses and distortion [7] as well as an anisotropic microstructure that results in the anisotropic material behavior [8]. Residual stresses and anisotropy occur due to the high cooling rates and directional dependency of the built process with numerous single melt tracks. The formation, the amount and the distribution of defects and residual stresses is highly dependent on the process parameters and consequently on the energy input and the interaction of the laser with the powder material in the process zone [9].

During the process the melt pool from the completely molten powder particles wets the previous solidified material. The wetting behavior of the melt is influenced by alloying elements but also from the oxygen coming from different sources like the gas atmosphere of the process including the trapped gas inside the powder bed or the powder material itself [10]. As the wetting of the surface with the liquid metal is hindered by oxide films, possible surface contamination of the previous layer and oxide films have to be removed with a sufficient amount of re-melting [9]. The oxide layers vaporize and the oxide particles are ejected from the process zone as fume [11]. Even with the low oxygen contents of the process atmosphere the formation of oxide compounds can be detected within the ejected spatter of the process zone [12]. In this work, the mechanical properties of LBM-generated tool steel 1.2344 for static and cyclical loading are investigated as well as the anisotropic material state regarding the overall oxygen content and its local distribution.

Experimental

Powder material out of tool steel 1.2344 with a spherical grain shape and grain sizes between 10 µm and 45 µm was used. The LBM-process was performed on a SLM Realizer 250 from Realizer GmbH (part of the DMG Mori AG). The machine employs a 200 W single mode fiber laser form IPG with a wavelength of 1073 nm. For the specimen fabrication Argon was used for the inert gas atmosphere. To reduce the occurrence of temperature gradients and induced residual stresses the substrate plate was preheated to 240 °C [13]. For the determination of the tensile and fatigue strength six tensile specimens and 19 fatigue specimens were produced with 100 W laser power, 100 mm/s scan speed and a horizontal build-up direction with a polar angle of 0°. The specimens were manufactured with a chessboard scan pattern with alternating tiles of 3 mm with a rotation of the complete pattern of 79° for every new layer. The specimens were post processed via turning. Six additional fatigue specimens were investigated on the influence of the LBM-surface. The specimens were fabricated with a stripes scan pattern with a stripe width of 10 mm. All produced specimens received no further heat treatment after the LBM-process.
The relative density of the material with the used process parameters was examined with a density determination kit YDK01 from Sartorius with a measurement according to Archimedes principle. The material's Vickers hardness (HV1) was measured with a LV-700 AT testing device from LECO. A 3D Laser Scanning Microscope VK-9700 from Keyence was used to determine the roughness by the arithmetical mean height Sa of the scale-limited surface. The tensile specimens were tested with an RM250 testing machine from Schenk. The fatigue specimens were tested with an electro-mechanical resonance testing machine from Amsler Type 2HFP with a load-controlled push-pull-test at a stress ratio of R = -1. The number of load cycles was limited to 10^7 load cycles and specimens, which did not fail until this limit, have been rated as run outs at this mark. The testing frequency was 125 Hz ± 10 Hz. In order to get more information on the possible causes of failure and the fracture probabilities the run-out specimens were tested again with increasing stress amplitudes until fracture. The cause of failure for every broken specimen was analyzed with scanning electron microscopy (SEM). The specimens were tested on different stress levels with one to four specimens per stress level according to the staircase method. The experimental fracture probability for each stress level was determined by the ratio of the number of fractured specimens to the number of tested specimens. The dependency of the fracture probability P_F on the stress amplitude S_a can be described with a two parametric Weibull distribution with the median of the fatigue strength S_F which represents the fatigue limit with a fracture probability of 50% and the Weibull coefficient m. The distribution (1) was fitted to the experimentally obtained fracture probabilities.

$$m_{\xi} = Z = NJ = O^{\left(p_{\sim}/p_c\right)^{\tilde{a}}} \tag{1}$$

The fatigue life of the fractured specimens with the turned surface and the specimens with a LBM-surface is described according to Basquin. The parameters S_0, N_0 are adopted to fatigue strength and k describes the slope of the fatigue life of the specimens (2).

$$k_{RM}(p_{\sim}) = Z = k_M \left(p_M/p_{\sim}\right)^{\hat{a}} \tag{2}$$

The oxygen content of the material and a fracture surface was analyzed in order to gain further insights on the material behavior and possible changes of the overall content as well as the distribution during the LBM-process. Therefore, measurements via inert gas fusion, energy-dispersive X-ray spectroscopy (EDX) and secondary-ion mass spectrometry (SIMS) were performed. The SIMS and EDX analysis were performed at the Fraunhofer IST in Braunschweig. The total oxygen and nitrogen contents of the powder and the solidified specimens from powder were measured via inert gas fusion with an ONH-2000 from ELTRA along with specimens out of conventionally fabricated 1.2344. A small amount of the powder material was melted directly in the furnace. The solid material was extracted from tensile test specimens for LBM-generated and conventionally fabricated material. The total contents were determined as the mean value of three individual measurements for the powder material and five for the solid materials respectively. The EDX and SIMS measurement were performed on the fracture surface of one fatigue specimen. The region of interest lies around the cause of failure within a lamellar structure in the steel matrix. For a qualitative comparison of the local oxygen distribution the measurements were also performed on two reference areas around the structure. The EDX-mapping and the SEM-images were done with 15 keV. The EDX-mapping was performed to classify the approximate oxygen quantity of the depth profiles of the SIMS-analysis. For the SIMS-measurement the specimen was exposed to primary Cs+ ions with an energy of 5 keV. The area of the screened surface was 400 µm × 565 µm. The ion beam hits the specimen in a 45° angle. The sputter rate on steel was 0.9 µm/h. The sputter time was 20 h and resulted in an 18 µm deep crater.

Results

The produced LBM specimens have a roughness Sa of 32 µm ± 7 µm for the LBM-surface without post processing. For specimens with a turned surface the average Sa is 3 µm ± 1 µm. The relative density of the generated material is above 99%. The average hardness values are 579 HV1 ± 15 HV1 and 571 HV1 ± 15 HV1 for the stripes pattern and the chess pattern respectively. All six tested tensile specimens have a similar stress-strain behavior, failing without constrictions and resulting in brittle fracture surfaces. The obtained average values are 892 MPa for the yield strength and 1440 MPa for the tensile strength. The average value for fracture elongation is 1.5%. The detailed tensile properties are given in **Table 1**.

Table 1 Tensile properties of LBM-generated 1.2344 specimens with chess scan pattern

	Yield Strength	Tensile Strength	Fracture Elongation
Mean value	892 MPa	1440 MPa	1.5%
Standard deviation	55.2 MPa	34.6 MPa	0.2%

The S-N diagram of the performed fatigue tests is displayed in **Figure 1**. The starting stress amplitude of the fatigue tests is 420 MPa, which is about half of the yield strength of the tensile specimens in consideration of the expected residual porosity of the specimens. The testing stress amplitude S_a of the turned specimens is within the range of 420 MPa and 280 MPa. The calculated fatigue strength S_F according to equation (1) is 283 MPa for 10^7 load cycles and a fracture probability P_F of 50%. The scatter m of the results is 3.4. The diagram shows the Basquin-curve of the data and culminates into the fatigue strength. The starting amplitude of the specimens with the LBM-surface is 200 MPa. All specimens of the batch fractured before the set limit of 10^7 load cycles. Due to the limited specimen number no statistical validated fatigue limit can be calculated for this specimen type. However, based on the fatigue data the approximated fatigue limit is below 100 MPa which is significantly lower than the fatigue strength of the turned specimens.

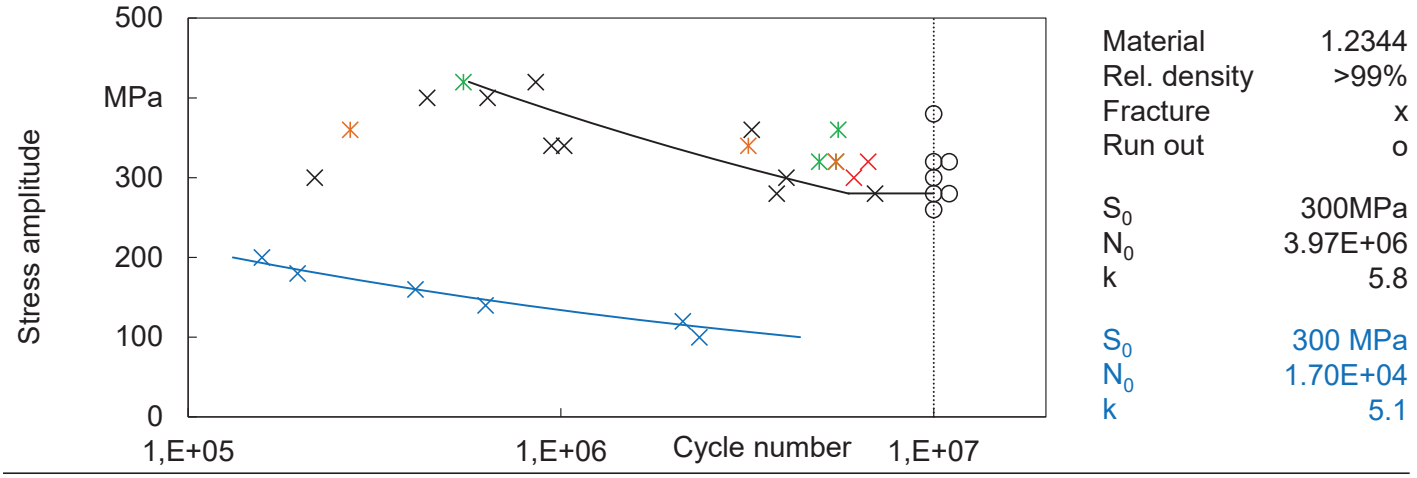

	Turned surface			LBM-surface
Fracture type	Fractured specimens	Run out specimens	All specimens	All specimes
Pore / cavity	10x	4*	14	
Matrix	2x	3*	5	
Surface				6x
Unknown		1 (Thread failure)	1	

Dörfert 2019, Data from IWT BIAS ID 190998

Figure 1 S-N-Diagram of LBM-generated specimens out of 1.2344 with different surface conditions and the corresponding fracture types

All the fractured fatigue specimens have a fractured surface perpendicular orientated to the loading direction but show different fracture types. For rough specimens the roughness peaks of the LBM-surface serve as notches and thus as crack initiation points. All six tested rough specimens have their critical defects on the surface itself. The high relative density of the specimens results in overall homogeneously distributed pores as critical defects for the turned specimens along with sporadically present cavities. The location of these critical defects is dominant near the surface and less present in the volume area. The third observed fracture type appears in the steel matrix itself and results in lamellar structures within the fracture surface for all specimens with this matrix failure. This fracture type cannot be allocated to specific pores that are still present inside the specimens. The distribution of the fracture types is also displayed in **Figure 1**. For 10 out of 19 tested specimens with the turned surface the cause of failure can be allocated to a present pore or cavity and two show the lamellar structure. Eight specimens achieved the 10^7 load cycles. The further testing of the run-out specimens results in additional failure in pores or cavities for four specimens and additional lamellar structures in the steel matrix for 3 specimens. One run out specimen failed at repeated test with increased stress amplitude in the thread. For that reason, the weak point of that specimen is unknown.

The mean values of the measured total contents of oxygen and nitrogen are displayed in **Table 2**. The oxygen and nitrogen content of the powder material is significantly higher compared to the conventionally fabricated material. The contents of the resulting LBM-parts are similar to that of the starting powder material. A measurement of reused powder shows no significant oxygen pick-up due to the process.

Table 2 Oxygen (O) and nitrogen(N) content measured via inert gas fusion

Material condition	O [ppm]	N [ppm]
Powder material (delivery status)	541	181
Powder material (reused batch)	623	187
LBM-generated material	569	368
Conventional material (annealed)	13	128

Figure 2 shows a SEM image of a distinct lamellar structure (S) on a fracture surface as well as the two surrounding reference areas (1 & 2) for the comparison before and after the SIMS-measurement of the specimen tested at S_a = 300 MPa and failed at 6.110.800 load cycles. The structure is completely ablated by the ion beam. The SEM image displayed in **Figure 3** indicates areas of the EDX-Mapping with Spectrum 1 indicating the area of the ion beam crater that includes the lamellar structure as well as the two reference areas 1 & 2 (which are displayed in **Figure 2**) and Spectrum 2 indicating an area around the crater that is not influenced by the ion beam. The EDX spectra is displayed in **Figure 4**. After the ablation of the structure the oxygen content is at 9.5 at% for Spectrum 1. The second measurement in the surrounding area shows 23.4 at% for the fracture surface with an oxide layer in Spectrum 2. The values are indicators for the approximate oxygen contents of the SIMS-depth-profile.

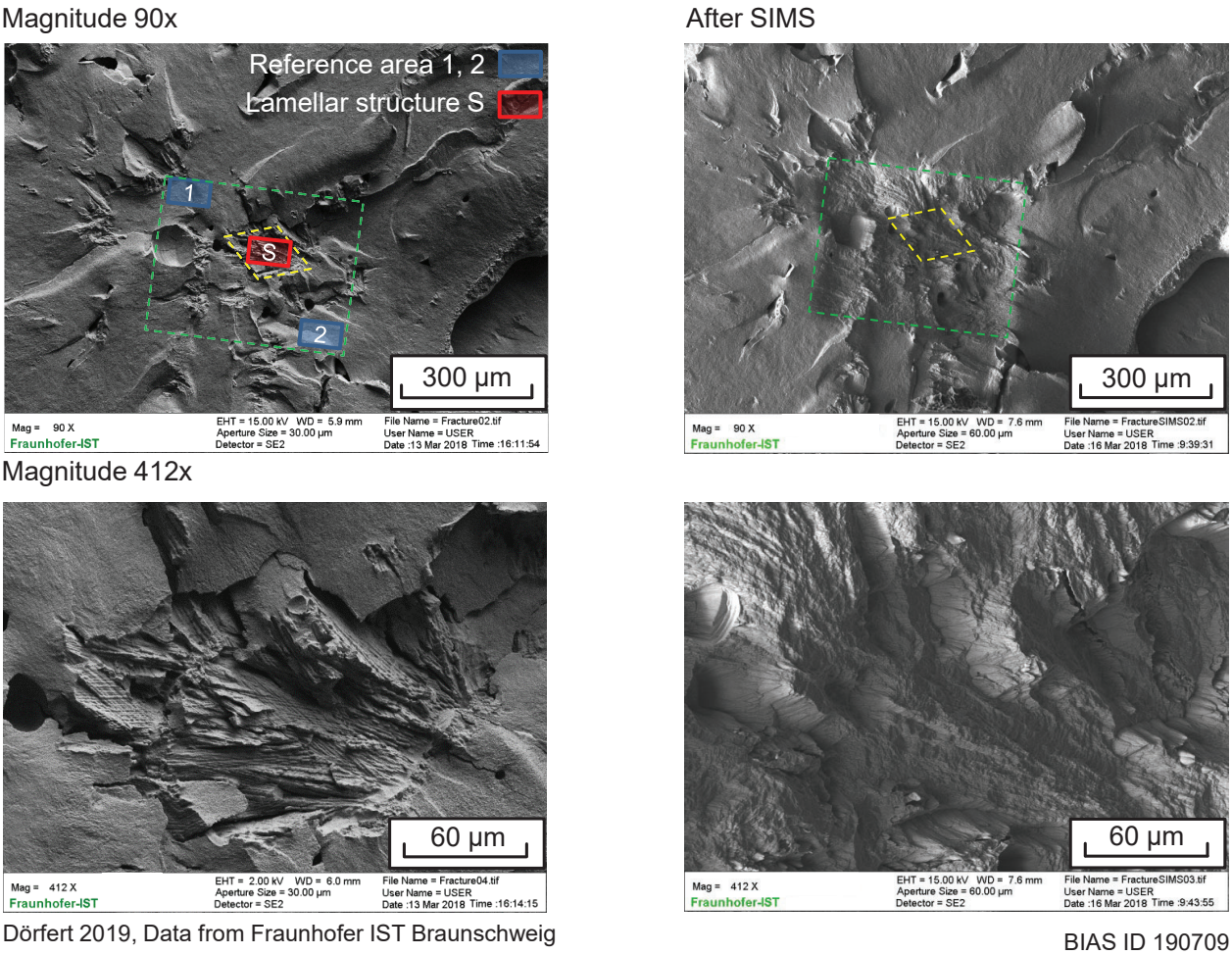

Figure 2 SEM images of the fracture surface before and after the SIMS-measurement with indications of the measuring points at the surrounding area (Reference area 1 & 2) for comparison and the lamellar structure (S)

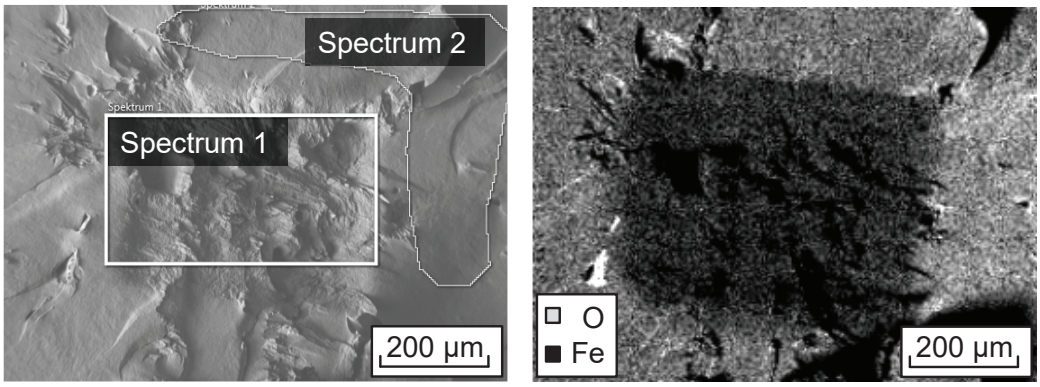

Dörfert 2019, Data from Fraunhofer IST Braunschweig

BIAS ID 190710

Figure 3 SEM-image (left) and EDX oxygen mapping (right) with 2 keV inside the ion beam crater (Spectrum 1) and outside of the crater (Spectrum 2)

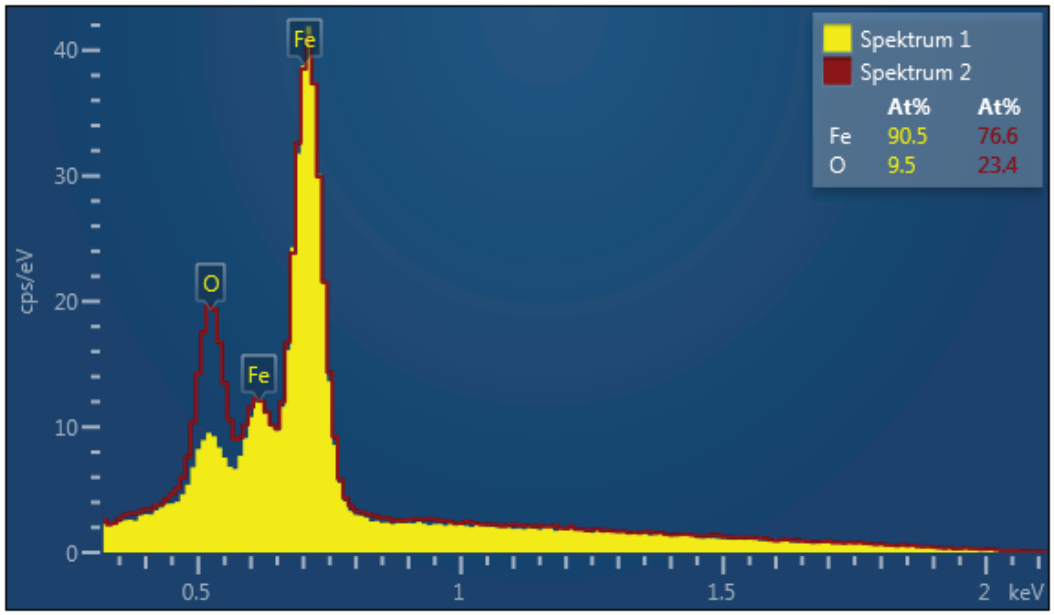

Figure 4 EDX spectra of Spectrum 1 and Spectrum 2

The SIMS-analysis in **Figure 5** shows the depth-profiles from 0 µm to 18 µm of the relative oxygen content on the structure and the two reference points in the surrounding area as shown in **Figure 2**. After the ablation of the oxide layer on the fracture surface the oxygen content reduces rapidly. The structure shows a plateau maximum up to a depth of 9 µm and decreases with further increasing depth. In comparison, the first reference area 1 outside of the structure has a continuously lower oxygen content whereas reference area 2 has an overall higher oxygen content. A more detailed distribution of the oxygen ions is displayed in **Figure 6** which is highly irregular. Areas with high oxygen contents are displayed red and areas with lower oxygen contents are displayed green. The area proportion of sections with a high oxygen content reduces significantly after the oxide layer of the surface is removed from the ion beam. With the increasing depth the distribution of the oxygen is still highly irregular and not limited to the structure as cause of failure. In addition, areas with a high oxygen content do not persist through the whole depth profile. During the ablation process local oxygen peaks disappear and new peaks appear in different locations of the measuring area.

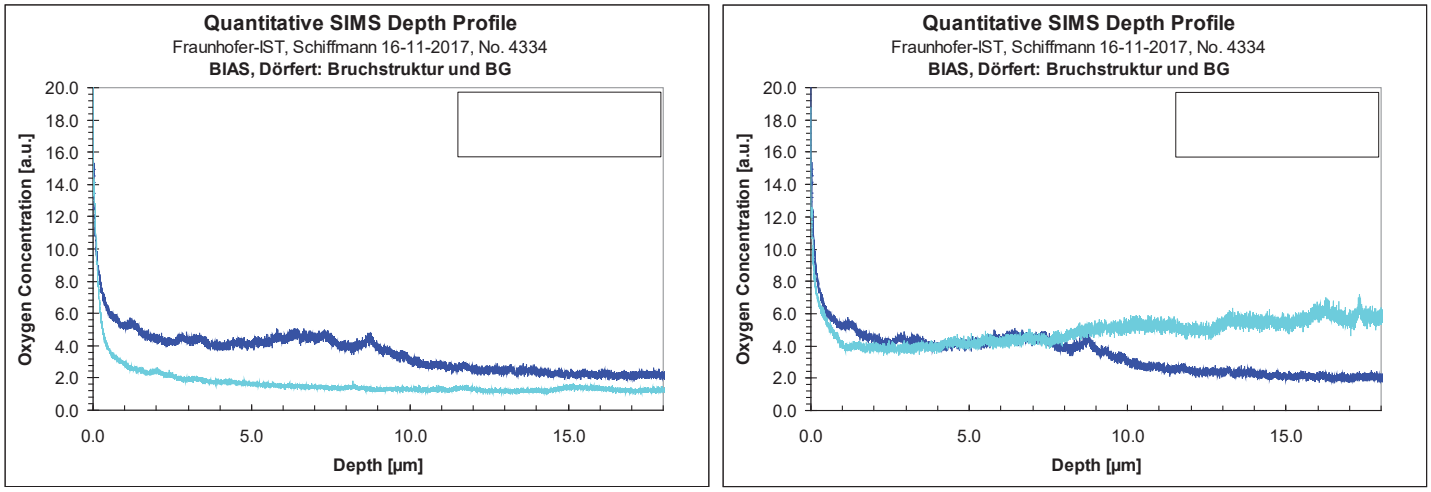

Figure 5 SIMS depth-profile of the oxygen signal for the area of the lamellar structure and two reference areas (1 & 2) located around the structure according to **Figure 2**

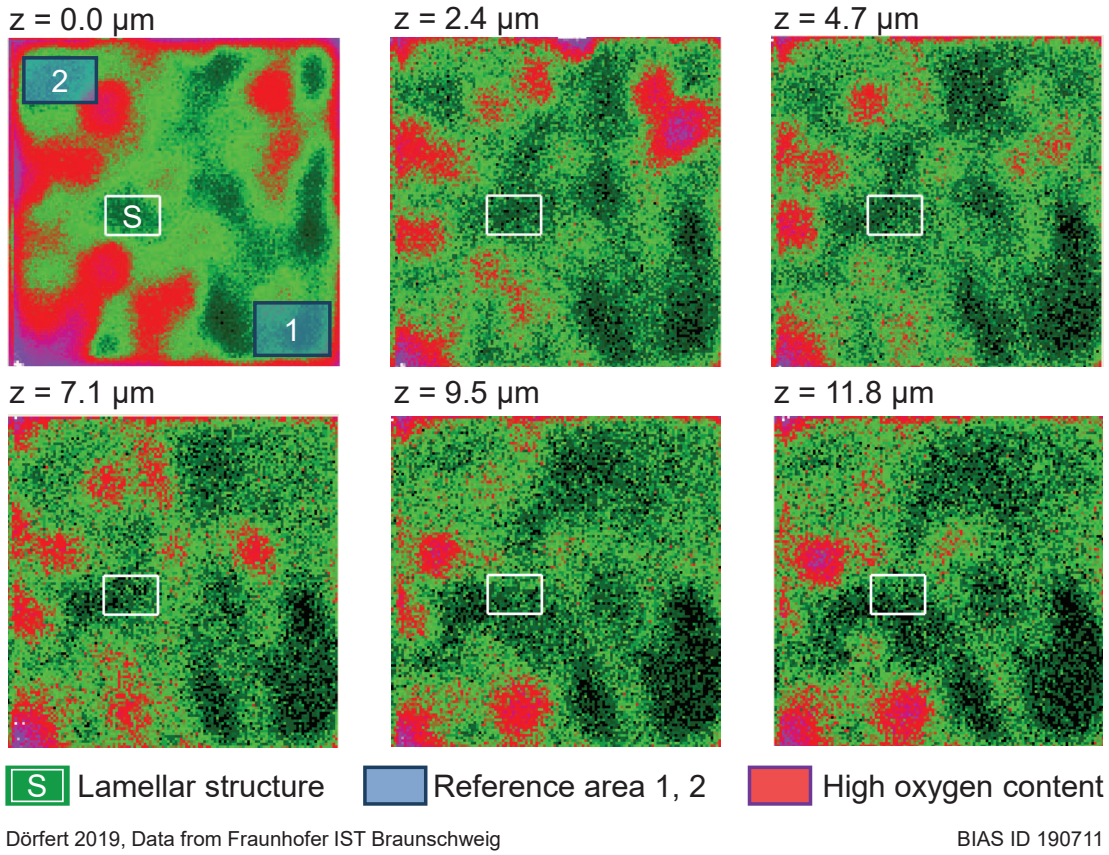

Figure 6 Oxygen ion distribution for different ablation depths from 0 µm to 11.8 µm with higher oxygen contents displayed red and lower oxygen contents displayed green (The ion image is turned by 180° in relation to the SEM-images from **Figure 2**)

Discussion

The mechanical properties for the LBM-generated 1.2344 showed without further heat treatment a tensile strength of 1440 MPa ± 32 MPa and an average hardness of 571 HV1 ± 15 HV1 which is within the range of conventionally fabricated and heat treated 1.2344 [14]. On the other hand, the mechanical properties for cyclical loading are significantly limited by the typically high surface roughness with a fatigue limit below 100 MPa and the characteristic residual porosity and defects with a fatigue limit of 283 MPa for this process. The roughness of the LBM-surface is the major impact factor on the fatigue strength due to the notch effects induced by the roughness peaks leading to high stress concentrations [5]. If the influence of the surface roughness is eliminated by post processing via turning the cause of failure shifts to the volume to the characteristic residual porosity of the process as well as local defects and cavities due to insufficient layer connection or powder solidification. Those defects can increase the local stress concentration especially if the defects are located near the surface. However, if the achieved relative density of the produced parts is high and not undermined by large cavities the cause of failure is not only found at single pores but also in the steel matrix itself. Thus, besides the generally regarded influence factors on the mechanical properties the condition of the microstructure of the material and the influence of the used powder material is of great interest. Compared to other forms of raw material like casted or forged material the powder material possesses a significantly larger surface area that leads to a high affinity for oxygen which can lead to the formation of oxide compounds on the particles surface if not completely isolated from the atmosphere [15]. A source for additional oxygen during the process is the process atmosphere. Despite the use of inert gas like Argon or Nitrogen the low oxygen content of the process atmosphere can still lead to further oxidization of the used powder. Oxides can also be found in spatters [12] or result in tarnish colors of the parts [16]. The analysis of the resulting oxygen contents of the produced LBM-parts shows a significantly higher amount of oxygen with 569 ppm compared to the conventional fabricated 1.2344 (annealed) with 13 ppm. However, the oxygen content is similar to the 541 ppm of the used powder material. Thus, the additional oxygen pick-up during the process through the atmosphere is presumably low. A clearer image of the qualitative oxygen distribution can be obtained with the SIMS-analysis of the fractured surface. The cause of failure for the analyzed specimen with the distinct lamellar structure lies in the steel matrix. The material shows a highly irregular oxygen distribution after the ablation of the oxide layer on the surface. The detected local concentrations of oxygen can be allocated to the fractured area around the cause of failure and are a further indication of the local oxide compounds that can induce higher stress concentrations and are part of the anisotropic behavior of LBM-generated material.

Conclusion

Additive manufactured parts with low porosity show, compared to bulk material, a weakness in fatigue strength. The fatigue strength level can be improved in the following order:

1. reducing the surface roughness,
2. reducing the residual porosity, and
3. reducing the oxygen content,

as the failure is induced by the respective faults. As the powder used for LBM has a high oxygen content, it is concluded that high (fatigue) strength parts can be generated, if a low porosity and deoxidation measures are implemented into the LBM process.

Acknowledgements

This work was funded by the Deutsche Forschungsgemeinschaft DFG (German research foundation) under contract no. 275999847 "Fatigue strength of by selective laser melting generated samples", which the authors gratefully acknowledge. The authors also like to thank Dr. Kirsten Schiffmann from Fraunhofer IST in Braunschweig for providing the SIMS-analysis.

References

[1] Schmidt, M., Merklein, M., Bourell, D., Dimitrov, D., Hausotte, T., Wegener, K., Overmeyer, L., Vollertsen, F., Levy, G.N., 2017. Laser based additive manufacturing in industry and academia. CIRP Annals 66 (2), 561–583.

[2] Kritzinger, W., Steinwender, A., Lumetzberger, S., Sihn, W., 2018. Impacts of Additive Manufacturing in Value Creation System. Procedia CIRP 72, 1518–1523.

[3] Spierings, A.B., Starr, T.L., Wegener, K., 2013. Fatigue performance of additive manufactured metallic parts. Rapid Prototyping Journal 19 (2), 88–94.

[4] Shrestha, R., Simsiriwong, J., Shamsaei, N., 2019. Fatigue behavior of additive manufactured 316L stainless steel parts: Effects of layer orientation and surface roughness. Additive Manufacturing 28, 23–38.

[5] Stoffregen, H.A., Butterweck, K., Abele, E., 2014. Fatigue Analysis in Selective Laser Melting: Review and Investigation of Thin-walled Actuator Housings. Solid Freeform Fabrication Symposium (SFFS).

[6] Riemer, A., Leuders, S., Thöne, M., Richard, H.A., Tröster, T., Niendorf, T., 2014. On the fatigue crack growth behavior in 316L stainless steel manufactured by selective laser melting. Engineering Fracture Mechanics 120, 15–25.

[7] Neugebauer, F., Keller, N., Ploshikhin, V., Feuerhahn, F., Koehler, H., 2014. Multi Scale FEM Simulation for Distortion Calculation in Additive Manufacturing of Hardening Stainless Steel. IWOTE.

[8] Edwards, P., Ramulu, M., 2014. Fatigue performance evaluation of selective laser melted Ti–6Al–4V. Materials Science and Engineering: A 598, 327–337.

[9] Kruth, J.-P., Froyen, L., van Vaerenbergh, J., Mercelis, P., Rombouts, M., Lauwers, B., 2004. Selective laser melting of iron-based powder. Journal of Materials Processing Technology 149 (1-3), 616–622.

[10] Kruth, J.-P., Levy, G., Klocke, F., Childs, T.H.C., 2007. Consolidation phenomena in laser and powder-bed based layered manufacturing. CIRP Annals 56 (2), 730–759.

[11] Louvis, E., Fox, P., Sutcliffe, C.J., 2011. Selective laser melting of aluminium components. Journal of Materials Processing Technology 211 (2), 275–284.

[12] Simonelli, M., Tuck, C., Aboulkhair, N.T., Maskery, I., Ashcroft, I., Wildman, R.D., Hague, R., 2015. A Study on the Laser Spatter and the Oxidation Reactions During Selective Laser Melting of 316L Stainless Steel, Al-Si10-Mg, and Ti-6Al-4V. Metall and Mat Trans A 46 (9), 3842–3851.

[13] Shiomi, M., Osakada, K., Nakamura, K., Yamashita, T., Abe, F., 2004. Residual Stress within Metallic Model Made by Selective Laser Melting Process. CIRP Annals 53 (1), 195–198.

[14] Mazur, M., Brincat, P., Leary, M., Brandt, M., 2017. Numerical and experimental evaluation of a conformally cooled H13 steel injection mould manufactured with selective laser melting. Int J Adv Manuf Technol 93 (1-4), 881–900.

[15] Seyda, V., 2018. Werkstoff- und Prozessverhalten von Metallpulvern in der laseradditiven Fertigung. Dissertation. Springer Berlin Heidelberg, Hamburg.

[16] Hauser, C., Childs, T.H.C., Dalgarno, K.W., Eane, R.B., 1999. Atmospheric Control during Direct Selective Laser Sintering of Stainless Steel 314S Powder. Solid Freeform Fabrication Symposium (SFFS).